

Spin-transfer torque induced spin waves in antiferromagnetic insulators

Matthew W. Daniels,^{1,*} Wei Guo,^{2,*} G. Malcolm Stocks,³ Di Xiao,^{1,†} and Jiang Xiao^{2,‡}

¹*Department of Physics, Carnegie Mellon University, Pittsburgh, Pennsylvania 15213, USA*

²*Department of Physics and State Key Laboratory of Surface Physics, Fudan University, Shanghai 200433, China*

³*Materials Science and Technology Division, Oak Ridge National Laboratory, Oak Ridge, Tennessee, 37831, USA*

We explore the possibility of exciting spin waves in insulating antiferromagnetic films by injecting spin current at the surface. We analyze both magnetically compensated and uncompensated interfaces. We find that the spin current induced spin-transfer torque can excite spin waves in insulating antiferromagnetic materials and that the chirality of the excited spin wave is determined by the polarization of the injected spin current. Furthermore, the presence of magnetic surface anisotropy can greatly increase the accessibility of these excitations.

I. INTRODUCTION

The field of spintronics seeks to investigate and organized phenomena concerning spin angular momentum. Of much recent interest in this field are spin-transfer torque (STT)^{2,3}, spin pumping,⁴ current-induced magnetization dynamics (spin waves),⁵ the (inverse) spin Hall effect,^{6,7} and the more recent spin caloritronics.⁸ As a scientific enterprise, this rich intersection of spintronic physics hosts a vast and non-trivial dynamical landscape with many yet-unexplored avenues of research. Meanwhile, the degree to which spintronics can be applied to problems in computational information architecture is already quite promising, and it is likely that the full extent of these technologies is presently unrealized. Spintronics as a technological program ultimately means to provide a high-information-density, energy-efficient computational architecture. STT and spin pumping provide a means to exchange spin into and out of a system, essentially constituting a I/O layer for applications. Therefore, their study is central in connecting any spin-based computing scheme to a realistic electronic device.

Over the past two decades, scientists expended considerable effort in learning to manipulate and detect ferromagnetic order via STT^{2,3} and spin pumping.⁴ This capacity to manipulate the magnetic order in ferromagnets—and, therefore, to initiate spin waves in the magnetic texture—is the foundation of *magnonics*. In the magnonics program, spin waves provide a complete replacement for itinerant electrons; information is no longer carried in conjunction with a flowing charge, but as a quasiparticle excitation of the background texture. The result is that no Joule heating is produced, making magnonics an attractive form of low-power computing. Recently, Kajiwara *et al.* have demonstrated the transmission of magnonics information, written and read via STT and spin pumping, in yttrium iron garnet (YIG).¹⁴ In their experiment, however, the critical current required to excite a spin wave was lower than expected. This discrepancy was later resolved by Xiao *et al.*, who theorized that the experimental apparatus had excited surface modes, rather than the expected bulk waves, and furthermore showed that these surface spin waves are associated with the considerably lower excita-

tion threshold found in the experimental data.⁴¹

Here, we are interested not in YIG, but in antiferromagnetic (AFM) magnonics. Because AFMs lack a net magnetization, their magnetic order is difficult to detect and control with magnetic fields. Applications of AFMs are consequently scarce, limited mostly to their use for exchange bias pinning of ferromagnets. Though spintronics research has historically focused on ferromagnetism, many theoretical works have considered how spin currents flowing through AFMs could interact with that magnetic order.^{15–23,25,26} These studies of spintronics in AFM metals, however, address the electron as the spin carrier. The ideal system for magnonics would be in an insulator, where magnons alone are the dominant spin carrier. But until recently, there existed a colloquial understanding that AFM insulators could not support magnons with a nonzero spin, for any spin carried on one sublattice would be canceled by the other.

Recently, Cheng *et al.* shattered this illusion by showing that, in easy-axis AFMs, spin waves necessarily carry a spin angular momentum by adopting either a left- or right-handed chiral mode.²⁷ Furthermore, they derived the magnetization dynamics due to STT in AFM insulators, and showed that both STT and spin pumping exist in AFMs and operate in a similar way to the ferromagnetic case. Despite these theoretical successes, some barriers still exist to realizing AFM magnonics in experiment. The most obvious dilemma is that, due to the strong exchange coupling in AFMs, the resonance frequency of bulk spin wave modes can be significantly higher than in ferromagnets—typically, it lies in the THz regime. Generating a THz signal is presently impossible by electronic means, as it would typically require a current which would melt the device before producing any meaningful effect.

In this article, we address the possibility of lowering the effective excitation threshold in AFM magnonics by considering the surface spin wave modes of AFMs. Our prediction relies on the fact that surface atoms in certain antiferromagnets can have an effective exchange energy significantly lower than the bulk value. One would then expect that the resonant frequency of spin waves localized to these exchange-reduced atomics will have lower excitation thresholds and be easier to excite. We com-

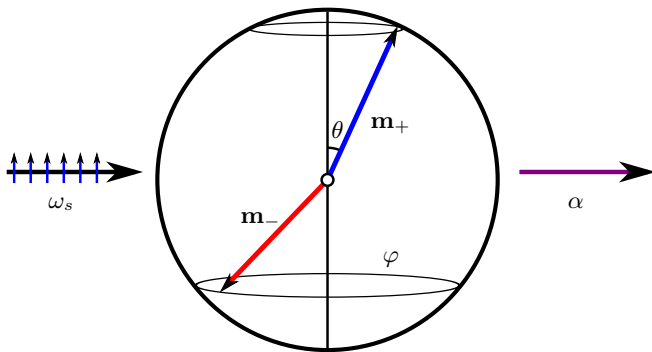


FIG. 1. (Color online) Cartoon setup for the macrospin model: two oppositely-oriented magnetic moments experience an exchange coupling ω_J via an on-site effective field. Spin-torque is injected via a polarized spin current ω_s , and energy is dissipated via the Gilbert damping α . Not pictured are the external field and uniaxial anisotropy, both along \hat{z} .

pute the surface spin wave spectra of antiferromagnetic insulators with both magnetically compensated and uncompensated surfaces, and show that these surface modes are, as expected, lower in energy. We then include a contribution from STT due to a polarized spin current injected at the surface. We find that this STT is sufficient to excite the surface spin waves in low-surface-exchange systems, which demonstrates a step toward making AFM magnonics more realizable in experiment. We also show that the sign of the STT determines the handedness of the chiral AFM spin wave as predicted by Cheng *et al.*²⁷

This paper is organized as follows: in Sec. II, we present a pedagogical model demonstrating not only that AFM spin waves can be excited by spin current, but also that the chirality of the spin wave depends on the spin current polarization. The distinction between source chiralities of spin waves due to their oppositely carried angular momentum could markedly improve the fidelity of devices utilizing the magnetization domain for information processing. In Sec. III, we make the system more realistic by extending the dynamical equations from two sites to a full cubic lattice. Here we present new results on AFM spin wave spectra for a semi-infinite system with an interface. Based on previous work,⁴¹ we expect that surface effects, by their role in modifying the magnons' activation threshold, will play an important part in the experimental realization of spin wave modes. In particular, we explore variations of the exchange coupling on the surfaces with both compensated and uncompensated net magnetizations. In Sec. IV, we offer concluding remarks and an application for experimental methods.

II. MACROSPIN MODEL

To provide a conceptual account of the mechanism underlying STT-generated spin waves in AF materials, we first present a minimal model which includes the impor-

tant physical terms without the complications of a spatially extended lattice. This so-called “macrospin model” has been considered by many in the past, and we include it here not as new work but as a pedagogical tool to illustrate the mechanism by which STT determines AFM spin wave handedness. We will then extend this idea to our core result on a semi-infinite lattice in Sec. III.

In the macrospin mode, the magnetization on the two sublattices are modeled as two macrospins,⁴² \mathbf{m}_+ and \mathbf{m}_- , which are coupled by a constant Heisenberg-type exchange interaction ω_J . They are additionally subject to Gilbert damping α and spin transfer torque ω_s ; the latter is due to an injected spin current polarized along the \hat{z} direction. Both macrospins experience the a uniaxial anisotropy ω_A in the \hat{z} direction.³⁶ We also allow for an external magnetic field $H_0\hat{z}$ along this axis. The setup is depicted schematically in Fig. 1, and yields an equation of motion

$$\begin{aligned} \dot{\mathbf{m}}_{\pm} &= -\mathbf{m}_{\pm} \times \mathbf{H}_{\text{eff}}^{\pm} + \alpha \mathbf{m}_{\pm} \times \dot{\mathbf{m}}_{\pm} + \omega_s \mathbf{m}_{\pm} \times (\hat{z} \times \mathbf{m}_{\pm}) \\ &= -\mathbf{m}_{\pm} \times [-\omega_J \mathbf{m}_{\mp} + (\omega_A m_{\pm,z} + \omega_H) \hat{z}] \\ &\quad + \alpha \mathbf{m}_{\pm} \times \dot{\mathbf{m}}_{\pm} + \omega_s \mathbf{m}_{\pm} \times (\hat{z} \times \mathbf{m}_{\pm}). \end{aligned} \quad (1)$$

where $\omega_H = \gamma H_0$. The effective field term $\mathbf{H}_{\text{eff}}^{\pm}$ is the negative derivative $-\nabla_{\mathbf{m}_{\pm}} H$ of the Hamiltonian

$$H = \omega_J \mathbf{m}_+ \cdot \mathbf{m}_- - \omega_H (m_+^z + m_-^z) - \frac{\omega_A}{2} (m_+^{z,2} + m_-^{z,2}) \quad (2)$$

where the damping term is added phenomenologically,⁴⁰ and the STT term—where ω_s is linear in the applied spin voltage—is due originally to Ref. 27; we partially rederive it for the reader in Appendix A.

In the small angle approximation, we demand that the deviation θ of $m_z \hat{z}$ from \mathbf{m} be small, so that $m_z = \cos \theta = 1 + O(\theta^2)$ and $m_{x,y} \propto \theta + O(\theta^3)$. Now the \hat{z} -component of equation Eq. (1) vanishes to order $O(\theta^2)$, and the problem is reduced to two effective dimensions in the xy -plane. We can exchange these two real dimensions for a single complex one by defining the transverse magnetization $u \equiv m_x + im_y$ and rewriting Eq. (1) in terms of this new variable. We then employ a spin wave *ansatz* $u_{\pm} = \mu_{\pm} e^{-i\omega t}$ which allows us to solve for the modes that satisfy equation Eq. (1). In the small-angle approximation, these eigenfrequencies of precession are

$$\omega_{\pm} = \pm\omega_0 - i\alpha(\omega_J + \omega_A) \left(1 \mp \frac{\omega_s}{\alpha\omega_0} \right). \quad (3)$$

The resonant frequency in the absence of damping and STT is $\omega_0 = \sqrt{\omega_A(\omega_A + 2\omega_J)}$. In AFM, two degenerate modes with opposite chirality appear in Eq. (3). This equation highlights the essential competition between STT and precessional damping: when the applied spin current is sufficiently strong, the second term in Eq. (3) becomes positive and selectively excites one of the ω_{\pm} modes depending on the sign of ω_s . Therefore, spin waves with different chirality can be selectively excited

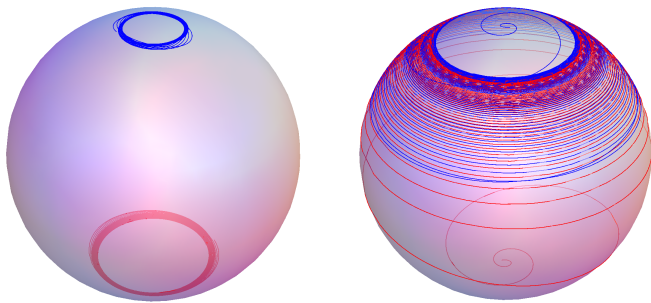


FIG. 2. (Color online) Left: With moderate ω_s which overcomes the damping effect, a stable oscillation AFM mode exists. This figure, which tracks the paths taken by spins \mathbf{m}_{\pm} from Fig. 1, is plotted for $t > 100$ after the system has neared its steady state oscillation. Right: with stronger ω_s , the system undergoes a spin flop, in which both \mathbf{m}_{\pm} tilt to the north hemisphere. For both figures, $\omega_A/\omega_J = 0.6$.

according to the spin current polarization. This behavior is different from STT-induced FM dynamics, for which only one polarization of spin current can excite FM spin waves while the other polarization enhances damping instead.

We can re-express \mathbf{m}_{\pm} in spherical angular coordinates $(\theta^{\pm}, \varphi^{\pm})$ and derive a set of exact, coupled ODEs for this system directly from the coupled LLG equations. θ^{\pm} is taken to be the polar angle between \mathbf{m}_{\pm} and \hat{z} , and φ^{\pm} is the corresponding azimuthal angle. We find

$$\dot{\theta}^+ = \omega_J \sin \Delta\varphi \sin \theta^- - (\alpha\dot{\varphi}^+ + \omega_s) \sin \theta^+ \quad (4a)$$

$$\dot{\varphi}^+ = \omega_H + \omega_A + \omega_J \sin \theta^- \cot \theta^+ \cos \Delta\varphi - \omega_J \cos \theta^- + \alpha\dot{\theta}^+ \csc \theta^+ \quad (4b)$$

$$\dot{\theta}^- = -\omega_J \sin \Delta\varphi \sin \theta^+ - (\alpha\dot{\varphi}^- + \omega_s) \sin \theta^- \quad (4c)$$

$$\dot{\varphi}^- = \omega_H - \omega_A + \omega_J \sin \theta^+ \cot \theta^- \cos \Delta\varphi - \omega_J \cos \theta^+ + \alpha\dot{\theta}^- \csc \theta^- \quad (4d)$$

where $\Delta\varphi = \varphi^+ - \varphi^-$. This result is analytically exact. Some numerical calculations for these ODEs are depicted in Fig. 2. Since the exchange energy is locally minimized where $\varphi^+ - \varphi^- = \Delta\varphi = \pi$, we expect $\dot{\varphi}^+ = \dot{\varphi}^-$. In the small angle approximation and neglecting $\dot{\theta}_{\pm}$ terms, this condition is satisfied when

$$\frac{\vartheta^+}{\vartheta^-} = - \left(\frac{\omega_J + \omega_A}{\omega_J \cos \Delta\varphi} \right) \pm \sqrt{\left(\frac{\omega_J + \omega_A}{\omega_J \cos \Delta\varphi} \right)^2 - 1}. \quad (5)$$

where ϑ^{\pm} are the angles that \mathbf{m}_{\pm} make with the $\pm\hat{z}$ axes. Choosing $\Delta\varphi = \pi$, as energetically expected, recovers the results from Ref. 36. Within the $\dot{\theta} \approx 0$ approximation, there is no real solution for $\vartheta^+ = \vartheta^-$ in the presence of easy-axis anisotropy, and one spin will always dominate the dynamics. Because the spins stay antiparallel, the two chiral modes correspond to a right-handed or left-handed rotation of the (+)-sublattice, and always carry a net angular momentum.²⁷

III. LATTICE CALCULATION

To consider a more realistic system than that of Sec. II, we now extend the Heisenberg-type Hamiltonian (2) to a simple cubic lattice as in Ref. 33:

$$H = \sum_{\langle i,j \rangle} \omega_{ij} \mathbf{m}_i \cdot \mathbf{m}_j - \sum_j \left(\omega_H + \frac{\omega_A}{2} m_{j,z} \right) m_{j,z}, \quad (6)$$

where the subscripts i and j are lattice sites and the first sum is taken over nearest neighbors.

We will consider both g - and a -type antiferromagnets. These configurations are depicted in Fig. 3, where the AFM terminates at $x = 0$ with compensated (left) and uncompensated (right) surfaces. We take the lattice constant as $a = 1$ so that the wavevector is dimensionless. The thermodynamic derivation from Sec. II is repeated for the Hamiltonian in Eq. (6) to derive an effective on-site magnetic field. Knowledge of this field determines the LLG equation for $\dot{\mathbf{m}}_j$, namely:

$$\dot{\mathbf{m}}_j = -\mathbf{m}_j \times \left[\sum_{\langle i,j \rangle} \omega_{ij} \mathbf{m}_i - (\omega_H - \omega_A m_{j,z}) \hat{z} \right] + \alpha \mathbf{m}_j \times \dot{\mathbf{m}}_j. \quad (7)$$

The exchange coefficients ω_{ij} will be uniformly constant $\omega_{ij} = \omega_J$ for the g -type system where all nearest neighbors are the same, though for the a -type system we will need to distinguish $\omega_{ij} = \omega_{\perp} < 0$ and $\omega_{ij} = \omega_{\parallel} > 0$ for the coupling between inter- and intra-plane (respectively AFM-like and FM-like) neighbors.

By assuming a small precession of \mathbf{m}_j about its easy-axis, the \hat{z} -component of the LLG Eqs. (7) can be neglected to first order. We then rewrite the equation of motion in terms of the transverse magnetization $u^{\pm} \equiv m_{\pm,x} + im_{\pm,y}$ as in Sec. II. Translational symmetry in time and the yz -plane validates the plane wave *ansatz*

$$u_{(j,s)}^{\pm} = \mu_{j,\mathbf{q}}^{\pm} e^{i(\mathbf{q}\cdot\mathbf{s} - \omega t)} \quad (8)$$

where j is the layer index in the \hat{x} -direction and \mathbf{q} is the wave vector in yz -plane. We substitute this equality into the transverse magnetization equation. From now on we will use \mathbf{k} to refer to a 3D wavevector and \mathbf{q} will be \mathbf{k} 's restriction in the yz -plane.

With these modifications, the LLG Eq. (7) is rewritten as a recurrence relation among different layers

$$S\psi_j + N_+\psi_{j+1} + N_-\psi_{j-1} = 0 \quad (9)$$

with $\psi_j = (\mu_j^+ \ \mu_j^-)^T$. The square matrices S , N_+ , and N_- can be computed directly from considering the coefficients in Eq. (7). For g -type,

$$S^{(g)} = \begin{pmatrix} \omega - \omega_H - \Omega & -\omega_q^{(g)} \\ \omega_q^{(g)} & \omega - \omega_H + \Omega \end{pmatrix}, \quad (10a)$$

$$N_+^{(g)} = N_-^{(g)} = \begin{pmatrix} 0 & -\omega_J \\ \omega_J & 0 \end{pmatrix} \quad (10b)$$

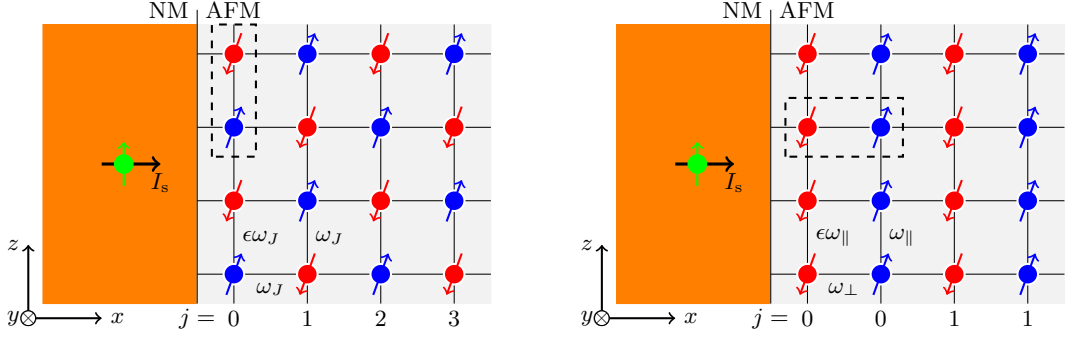


FIG. 3. (Color online) 2D slices of the spin configurations for g -type (left) and a -type (right) AFM, interfacing with NM. For g -type, the neighboring spins in the bulk have exchange coupling ω_J , but have coupling $\epsilon\omega_J$ on the surface. For a -type, the intralayer exchange coupling is ω_{\parallel} in the bulk and $\epsilon\omega_{\parallel}$ on the surface, while the interlayer exchange coupling is ω_{\perp} . In both cases, the far left column of spins is the $x = j = 0$ atomic surface layer which sits against a nonmagnetic interface. Unit cells are outlined in dashed box. Spin current I_s is injected from NM and exerting a torque on the surface spins.

with $\Omega = 6\omega_J + \omega_A - i\alpha\omega$ and $\omega_q^{(g)} = 2\omega_J (\cos q_y + \cos q_z)$. For a -type,

$$S^{(a)} = \begin{pmatrix} \omega - \omega_H - \Omega_q & -\omega_{\perp} \\ \omega_{\perp} & \omega - \omega_H + \Omega_q \end{pmatrix}, \quad (11a)$$

$$N_+^{(a)} = \begin{pmatrix} 0 & -\omega_{\perp} \\ 0 & 0 \end{pmatrix}, \quad N_-^{(a)} = \begin{pmatrix} 0 & 0 \\ \omega_{\perp} & 0 \end{pmatrix} \quad (11b)$$

with $\Omega_q = 2\omega_{\perp} + \omega_A + \omega_q^{(a)} - i\alpha\omega$ and $\omega_q^{(a)} = 2\omega_{\parallel} (2 - \cos q_y - \cos q_z)$.

A. Bulk calculation

For comparison with our results for a semi-infinite lattice in Sec. III B, we pause to reproduce the bulk spin wave spectrum this formalism. The reader may refer to Ref. 33, or to any condensed matter theory textbook, for a more complete discussion of the g -type spectral calculation. The a -type calculation is similar except that the primitive lattice vectors differ.

In addition to the translational symmetries used in the previous section, a bulk lattice possesses an additional translational symmetry in the \hat{x} direction. Therefore we may take a plane wave solution for the x -coordinate: $\psi_j = \phi(q)e^{i(k_x j - \omega t)}$. We can then find the eigenfrequencies of AFM spin waves. For g -type,

$$\omega_{(g)} = \omega_H \pm \sqrt{\Omega^2 - \omega_k^2} \quad (12)$$

with $\omega_k = 2\omega_J (\cos k_x + \cos k_y + \cos k_z)$. For the a -type lattice, we have an infinite stack of alternating ferromagnetic sheets. We choose for \hat{x} to be the direction normal to any given sheet. Then the bulk dispersion is

$$\omega_{(a)} = \omega_H \pm \sqrt{\Omega_q^2 - 4\omega_{\perp}^2 \cos^2 k_x}. \quad (13)$$

One can verify that in the limit $\omega_{\perp} = 0$ we recover decoupled 1D AF chains with the expected dispersion

$\pm 2\omega_{\perp} |\sin k_x|$ in the simple isotropic case.⁴³ Likewise, the $\omega_{\perp} = 0$ limit recovers a decoupled 2D ferromagnetic system, with dispersion $\pm 2\omega_{\parallel} |\cos k_y + \cos k_z - 2|$ in the same simple case.

The spin wave eigenfunctions corresponding to Eqs. (12,13) are respectively

$$\varphi_{\pm}^{(g)} = \begin{pmatrix} \sqrt{\Omega + (\omega - \omega_H)} \\ \mp \sqrt{\Omega - (\omega - \omega_H)} \end{pmatrix}, \quad (14a)$$

$$\text{and } \varphi_{\pm}^{(a)} = \begin{pmatrix} e^{ik_x} \sqrt{\Omega \pm (\omega - \omega_H)} \\ -\sqrt{\Omega \mp (\omega - \omega_H)} \end{pmatrix}. \quad (14b)$$

The dispersion relations (12,13) enforce a constraint linking the irreducible representations of time (ω) and space (k) translational symmetries. For any particular ω and \mathbf{q} , there are only a finite number of k_x values in its preimage under the eigenvalue Eqs. (12,13). In the next section, we will need to consider linear combinations of bulk solutions to satisfy the boundary condition. The dispersion relations above will allow us to consider only a small subset of all conceivable wavenumbers k_x .

B. The semi-infinite case

We now introduce an interface by terminating the insulator along its (100) plane and replacing the space $x < 0$ with a nonmagnetic contact from which spin current can be injected. We will modify the equations of motion to allow for special conditions on the atomic surface layer at $x = 0$.

First, an enhanced damping term is inserted into the LLG equation by taking $\alpha \mapsto \alpha + \beta\delta_{j\pm,0}$, where β is the enhanced damping parameter for the surface spins. This enhanced damping represents spin loss due to the spin pumping effect from the AFM back into the NM contact. The STT term $\omega_s \mathbf{m}_j \times (\hat{\mathbf{z}} \times \mathbf{m}_j) \delta_{j\pm,0}$ is likewise included on the atomic surface layer. Finally, as a form of surface anisotropy, we allow a modulation of

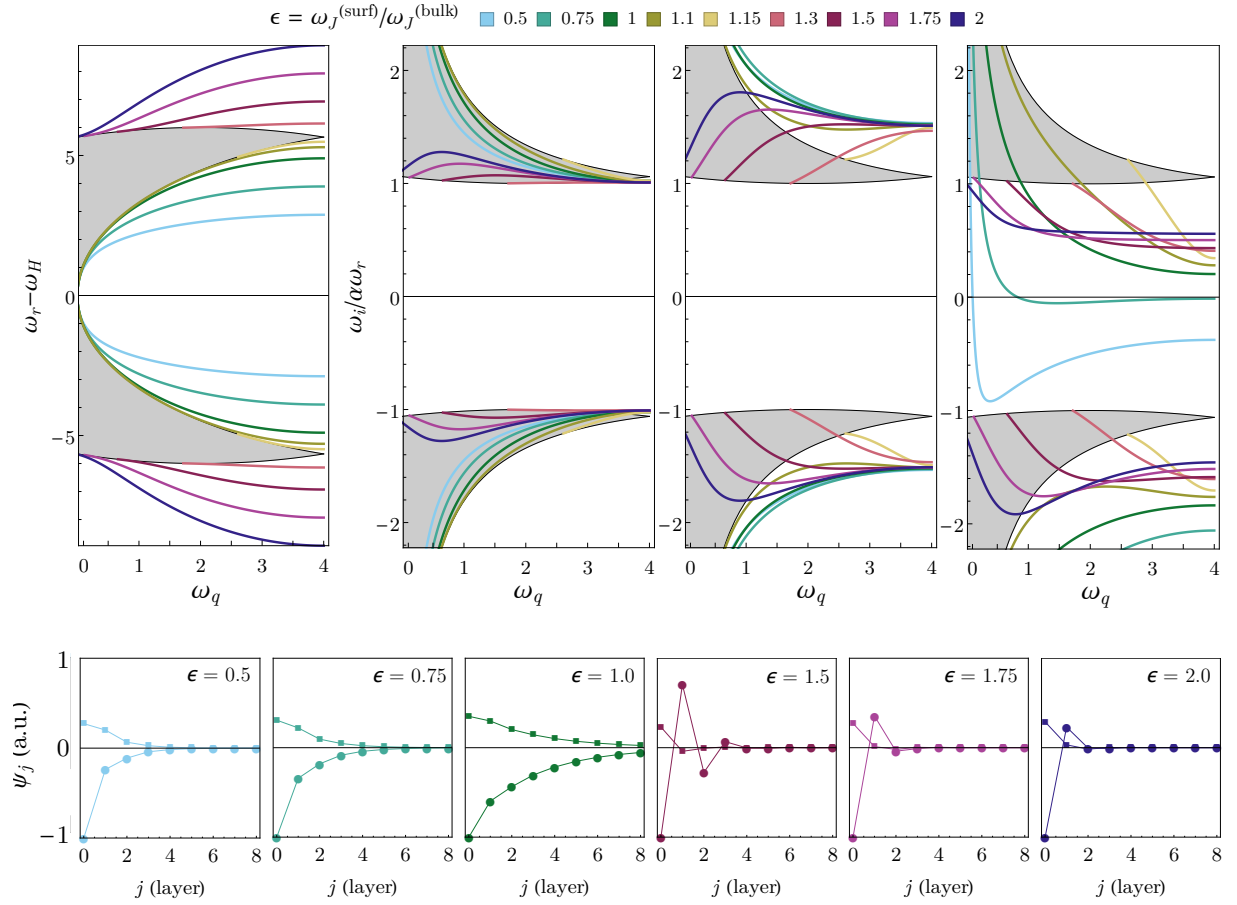


FIG. 4. (Color online) Frequency dispersion for the g -type semi-infinite system. From top left to top right: ω_r and then $\omega_i/\alpha\omega_r$ for $\alpha = 0.01$; $\alpha = 0.01$ and $\beta = \alpha/2$; $\alpha = 0.01$ and $\omega_s = 4\alpha$. The gray regions indicate the bulk spectrum. The horizontal axes measure $\omega_q \equiv 4 - \omega_q^{(g)}$, so that $\omega_q = 0$ corresponds to the Γ point in the surface Brillouin zone. An array of spin wave profiles plotting the magnitudes of ψ_j^\pm at $4 - \omega_q^{(g)} = 1.5$ is shown in the bottom row.

the intralayer exchange coupling represented by the ratio $\epsilon \equiv \omega_j^{\text{surf}}/\omega_j^{\text{bulk}}$ (or $\omega_{\parallel}^{\text{surf}}/\omega_{\parallel}^{\text{bulk}}$). It is known that this type of surface anisotropy can induce surface spin wave modes in AFM.³³ The variation in the exchange energy at the interface of magnetic materials has been studied by many groups. For instance, numerical studies on NiO(100) interfaces have shown that, depending on the assumptions of the model, surface exchange energy can vary by at least 20% with some groups showing as much as a 50% variation⁴⁴ from the bulk coupling.

We can write new equations of motion for this semi-infinite system as:

$$(S + B)\psi_0 + N_+\psi_1 = 0 \quad (j = 0) \quad (15a)$$

$$S\psi_j + N_+\psi_{j+1} + N_-\psi_{j-1} = 0 \quad (j > 0) \quad (15b)$$

where, for g - and a -types, respectively:

$$B^{(g)} = [(5 - 4\epsilon)\omega_J + i(\omega_s + \beta\omega)]\sigma_z + \omega_q(1 - \epsilon)i\sigma_y, \quad (16a)$$

$$B^{(a)} = -[\omega_{\perp} + \omega_q(1 - \epsilon) - i(\omega_s - \beta\omega)]\frac{1 - \sigma_z}{2}, \quad (16b)$$

and $\sigma_{x,y,z}$ are the Pauli matrices.

We now take the bulk eigenvectors φ_{\pm} in Eq. (14) for the g -type as a basis for general solutions to a semi-infinite lattice configuration. By using the bulk dispersion relations, φ_{\pm} can be rewritten in terms of a distinguished eigenvalue ω and trigonometric functions of k_x as in Eq. (14). Recall from the conclusion of Section III A that for a particular value of $\omega = \omega(\mathbf{q})$ the irreducible representation k_x is restricted to the finite set of values $k_x \in \omega_{(g,a)}^{-1}(\omega(\mathbf{q}))$. We will call these at most four values by k_{μ} . Since the cosine function is even, we see that two of the k_{μ} values are related by a sign change to the other two. As will become clear in Sections III B 1 and III B 2, we demand that $\Im(k_x)$ be positive so that surface solutions decay into the bulk. Then two allowed values of k_{μ} remain, which we call k^+ and k^- .

We can now consider solutions of the form

$$\psi_j = \eta_+\varphi_+e^{i(k^+j-\omega t)} + \eta_-\varphi_-e^{i(k^-j-\omega t)} \quad (17)$$

where φ_{\pm} are the bulk eigenvectors corresponding to k^{\pm} , which are the only allowed wavenumbers k_x in the preim-

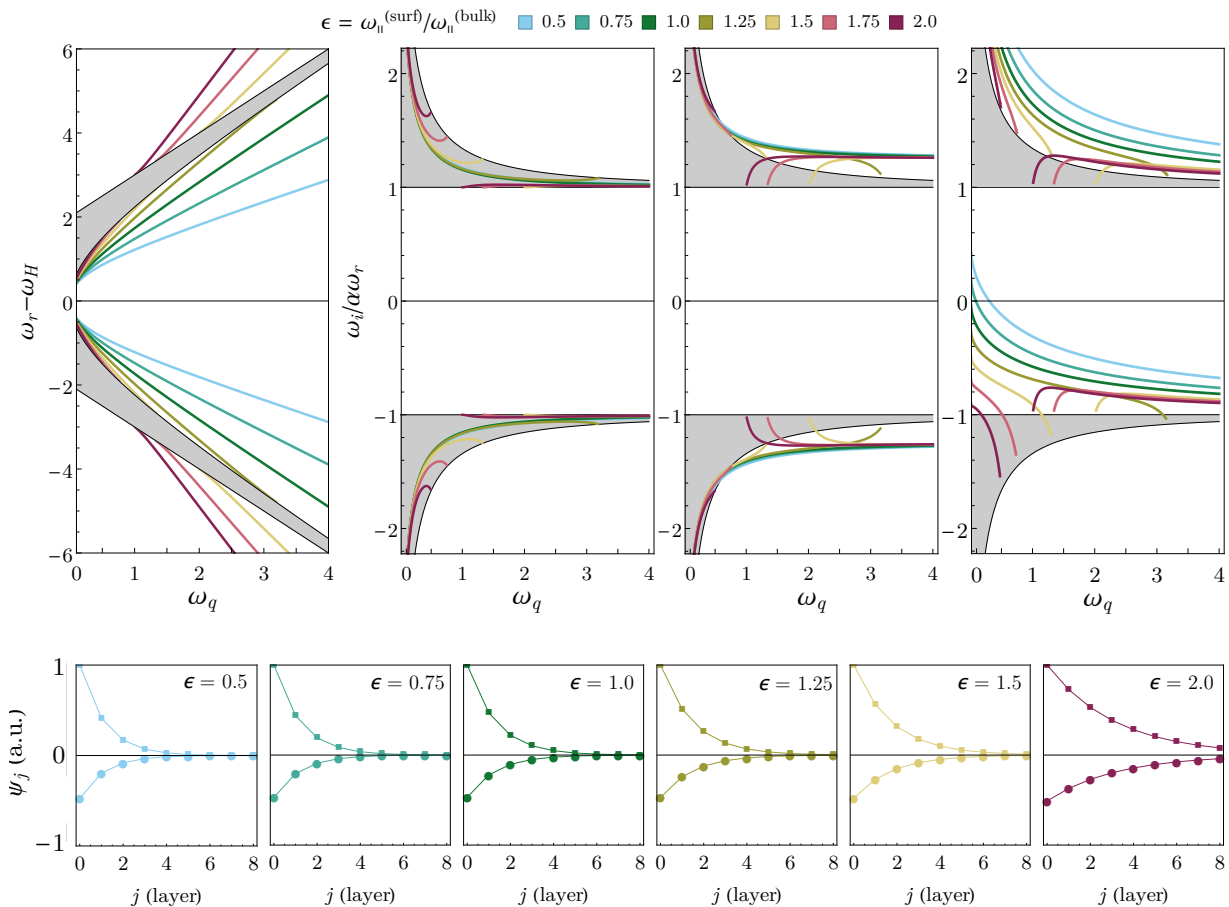


FIG. 5. (Color online) Frequency dispersion for the *a*-type semi-infinite system with $(\omega_{\parallel}, \omega_{\perp}) = (0.5, 1)$. From left to right: ω_r and then $\omega_i/\alpha\omega_r$ for $\alpha = 0.01$; $\alpha = 0.01$ and $\beta = \alpha/4$; $\alpha = 0.01$ and $\omega_s = \alpha$. The gray regions indicate the bulk spectrum. The horizontal axes measure $\omega_q \equiv \omega_q^{(a)}$, so that $\omega_q = 0$ corresponds to the Γ point in the surface Brillouin zone. An array of spin wave profiles plotting the magnitudes of ψ_j^{\pm} at $\omega_q^{(a)} = 0.3$ is shown below.

age of the bulk ω .

1. *g*-type, with compensated surface

With Eq. (17), the boundary condition Eq. (15a) for the compensated *g*-type system takes the form

$$\det \left[B(\varphi_+ \varphi_-) + N \left(\varphi_+ e^{ik^+} \varphi_- e^{ik^-} \right) \right] = 0. \quad (18)$$

The exponentials $e^{ik^{\pm}}$ can be determined from solving the eigenvalue equations Eq. (12,13) for $\cos k_x$, employing the Pythagorean identity to expand Euler's formula, and demanding solutions $\Im(k_x) > 0$ which decay into the bulk. Taken together with Eq. (12), this equation can be solved analytically for ω when $\alpha = \beta = \omega_s = 0$. This unperturbed eigenfrequency is then used to calculate constant perturbations—namely the $i\alpha\omega$ and $\beta\omega$ terms—so that equation Eq. (18) can be evaluated to leading order in the presence of damping and STT with straightforward modifications to its coefficients. The results in the com-

plex eigenfrequencies $\omega = \omega_r + i\omega_i$ are plotted in Fig. 4, wherein the bulk modes are plotted as the shaded area and the surface modes are plotted in colored curves. To the leftmost panel of Fig. 4 corresponds the real part of the eigenfrequency $\omega_r - \omega_H$ (in units of ω_J), and the right three panels are the imaginary part $\omega_i/\alpha\omega_r$ for three different cases: purely intrinsic damping, with neither spin pumping nor STT; both damping and spin pumping (due to the enhanced damping, β), but no STT; and both damping and STT, but no spin pumping.

The dispersion relations of ω_r for the surface modes of this system are plotted in Fig. 4 over a spectrum of surface exchange ratios ϵ . These surface modes are the same as those calculated in Ref. 33. The spin wave profiles for the surface modes are presented in lower panels of the figure, which shows a positive correlation between surface localization and surface anisotropy. These figures also reveal that the surface modes in a *g*-type AFM can be either acoustic or optical; a detailed discussion of the acoustic/optical transition as a function of ϵ is given in Ref. 33.

Beyond the dispersion relations, we are also interested in the dissipative behavior of various spin wave modes. Especially of interest are their behavior under the influence a STT due to spin current injection from the NM contact. The second panel of Fig. 4 shows ω_i when there is only intrinsic damping included. In this case there is neither spin pumping or STT, and we plot both the bulk modes (shaded continuum) and the surface modes (colored curves) for different values of the surface anisotropy ϵ . With the additional NM contact at the surface, the spin pumping into NM from AFM increases the dissipation for the spin wave modes, as seen in the third panel in Fig. 4. Far from where the surface modes emerge from the bulk spectrum, the effective damping enhancement (in the language of Ref. 24) is $\Delta\alpha \approx \beta$. This is expected since this regime corresponds to high surface localization, wherein β is effectively just added to α in the local LLG equations. introduction of a spin-transfer torque can dramatically decrease the damping of some surface spin waves, especially in the low- ϵ regime where surface anisotropy is strong. The low damping combined with low excitation energy makes these low- ϵ modes particularly excitable due to strong surface localization. Strong enough ω_s together with low ϵ (strong surface anisotropy) can cause sign changes in ω_i and lead to AFM spin wave excitation, as in the last panel of Fig. 4. Furthermore, STT distinguishes the two spin wave chiralities by enhancing the damping of one while reducing the other. Precisely which chirality is excited depends on the spin current polarization, so that it is distinctly possible to selectively excite a particular chiral mode.

2. *a*-type, with uncompensated surface

For the uncompensated surface in an *a*-type AFM insulator, there is effectively only one k_x which satisfies both the bulk eigenfrequency equations and the reality condition $\Im(k_x) > 0$ for any given ω . The reasoning follows: first, the orientation of the unit cell is necessarily different in the *a*-type system, so that the coupling to the next unit cell along the *x*-direction requires a factor of e^{2ik} rather than just e^{ik} in the *a*-type analog to equation Eq. (17); second, solving equation Eq. (13) for k_x gives a family of four solutions—namely k , $-k$, $\pi + k$, and $\pi - k$ —but as we mentioned in Sec. III B, only one of k and $-k$ will have a positive imaginary part, and they furthermore will each appear identical to their π -shifted partners when expressed in the form e^{2ik} . This simplifies the form of the boundary condition Eq. (15a), as well as the *a*-type analog of Eq. (18). A similar procedure to that employed in the previous section is used to solve the unperturbed and then perturbed versions of this equation.

The spin wave dispersion ω_r for an *a*-type AFM is different from that for *g*-type AFM; this is evident in the left panel of Fig. 5. However, the surface anisotropy still induces surface spin wave modes. Typical surface mode

profile are shown below the dispersion plots. In the absorption spectra (right three panels of Fig. 5), the spin pumping (third panel) enhances the dissipation for both chiralities (again at $\Delta\alpha \approx \beta$) while STT reduces the dissipation for one chirality and enhances the other. These results coincide with the outcomes of Section III B 1 for the *g*-type configuration, again distinguishing spin wave chiralities and demonstrating that a nonzero ω_s in the *a*-type system can cause a change in sign of the absorption spectrum, and can consequently excite spin wave modes.

IV. CONCLUSIONS

In this article, we have calculated the spin wave spectrum of STT-induced AFM surface excitations. In particular, we found that surface spin wave modes induced by surface anisotropy are particularly easy to excite compared to bulk modes, implying a lowering of the naive critical current needed to perform magnonic operations in AFM insulators.

As we noted in the Introduction, the efficiency of spin pumping processes in antiferromagnets is known to be comparable to their ferromagnetic cousins.²⁷ However, because antiferromagnets have a much stronger exchange coupling, an *a priori* estimate of the threshold current for exciting AFM surface spin waves is two to three orders of magnitude higher than in ferromagnet insulators. Nevertheless, the critical current for exciting a ferromagnetic magnon current was found in Ref. 14 to be two to three orders of magnitude lower than the expectation accorded to YIG's resonant frequency. If the same unforeseen reduction occurs in AFM, then the critical current would be on the order $J_c \approx 10^8 \text{ A/cm}^2$, which is within experimental feasibility. Our contribution is to take a first step in investigating this potential reduction in the critical barrier. One may of course seek materials with appropriate exchange or anisotropy energies in accordance with Eq. (3) in order to lower the barrier; we find that seeking materials with low surface exchange coupling reduces the threshold further.

Our work also takes a first step toward developing new experimental techniques for investigating antiferromagnets. Because it is relatively straightforward to generate a spin current and measure spin waves, STT-based methods could provide a new tool for probing and controlling AF materials. In particular, parameters such as damping, anisotropy, or surface exchange coupling could be inferred by retrofitting experimental data to models like those we present here. Since this data would be obtained by purely electrical means via a polarized spin current, it could be considerably easier to collect than neutron scattering results. Such a method could be a powerful complement to current experimental procedures, but is intractable without an understanding of the spin wave response to surface STT akin to that which we have outlined above. In any case, such a scheme would require considerable refinement to what we have presented here;

one would want to keep higher order terms, introduce another thin-film boundary, and break translational invariance along the surface. Treating non-single-crystal AFMs would introduce even more complication. We leave these details to future research, noting here only that continual improvement of our understanding of AFM spin waves should begin to open new routes to experimental investigation on the topic.

This work was supported by the National Science Foundation, Office of Emerging Frontiers in Research and Innovation EFRI-1433496 (M.W.D), the U.S. Department of Energy, Office of Basic Energy Sciences, Materials Sciences and Engineering Division (D.X. and G.M.S.), and by the special funds for the Major State Basic Research Project of China (grants No. 2014CB921600, No. 2011CB925601) and the National Natural Science Foundation of China (grant No. 91121002) (W.G. and J.X.).

Appendix A: Spin-transfer torque on AFM

In Sec. II we presented an extended LLG equation of motion which included a spin-transfer torque term induced by a \hat{z} -polarized spin current: $\tau_{\pm} = \omega_s \mathbf{m}_{\pm} \times (\hat{z} \times \mathbf{m}_{\pm})$. This form of term is plausible on the grounds of right-hand-rule gymnastics, but in this appendix we provide a more rigorous derivation of its physical content.

We begin from Eqs. (6) of Ref. 27, which provide the STT on the \mathbf{m} (magnetization) and \mathbf{n} (staggered) sublattices due to an applied spin voltage \mathbf{V}_s ,

$$\tau_n = -\frac{a^3}{e\mathcal{V}} G_r \mathbf{n} \times (\mathbf{m} \times \mathbf{V}_s) \quad (\text{A1})$$

$$\tau_m = -\frac{a^3}{e\mathcal{V}} G_r \mathbf{n} \times (\mathbf{n} \times \mathbf{V}_s) \quad (\text{A2})$$

where \mathcal{V} is the volume of the system, a is the lattice constant, and G_r is the real part of the spin mixing conductance for an NM|AFM interface; the corresponding imaginary part of G is several orders of magnitudes smaller²⁷ and consequently ignored. By definition, we have $\mathbf{m}_{\pm} = \mathbf{m} \pm \mathbf{n}$ on the two sublattices from Sec. II. Thus $\tau_{\pm} = \tau_m \pm \tau_n$, and the use of Eqs. (A1,A2) gives

$$\tau_{\pm} = -\frac{a^3}{e\mathcal{V}} \mathbf{n} \times (\pm G_r \mathbf{m}_{\pm} \times \mathbf{V}_s). \quad (\text{A3})$$

Now, as in the main text, we take the spin voltage to be collinear with the easy-axis \hat{z} : $\mathbf{V}_s = V_s \hat{z}$. Allowing $\mathbf{n} \approx 2\mathbf{m}_+ \approx -2\mathbf{m}_-$, we have

$$\tau_{\pm} = \frac{a^3 V_s}{e\mathcal{V}} G_r \mathbf{m}_{\pm} \times (\hat{z} \times \mathbf{m}_{\pm}), \quad (\text{A4})$$

and we define the relevant constant of proportionality as $\omega_s = (a^3 V_s / e\mathcal{V}) G_r$, thus achieving the form exhibited in equation Eq. (1).

* These authors contributed equally.

† dixiao@cmu.edu

‡ xiaojiang@fudan.edu.cn

¹ F. Pulizzi, Nature Materials **11**, 367 (2012).

² J. C. Slonczewski, Journal of Magnetism and Magnetic Materials **159**, L1 (1996).

³ L. Berger, Phys. Rev. B **54**, 9353 (1996).

⁴ Y. Tserkovnyak, A. Brataas, and G. E. W. Bauer, Phys. Rev. Lett. **88**, 117601 (2002).

⁵ S. I. Kiselev, J. C. Sankey, I. N. Krivorotov, N. C. Emley, R. J. Schoelkopf, R. A. Buhrman, and D. C. Ralph, Nature **425**, 380 (2003).

⁶ M. I. Dyakonov and V. I. Perel, ZhETF Pisma Redaktsiui **13**, 657 (1971).

⁷ J. E. Hirsch, Phys. Rev. Lett. **83**, 1834 (1999).

⁸ K. Uchida, S. Takahashi, K. Harii, J. Ieda, W. Koshibae, K. Ando, S. Maekawa, and E. Saitoh, Nature **455**, 778 (2008).

⁹ D. Pesin and A. H. MacDonald, Nature Mater **11**, 409 (2012).

¹⁰ W. Gerlach and O. Stern, Z. Physik **9**, 353 (1922).

¹¹ W. H. Meiklejohn and C. P. Bean, Phys. Rev. **105**, 904 (1957).

¹² A. A. Serga, A. V. Chumak, and B. Hillebrands, J. Phys. D: Appl. Phys. **43**, 264002 (2010).

¹³ S. O. Demokritov and A. N. Slavin, *Magnonics: From Fundamentals to Applications* (Springer Science & Business Media, 2012).

¹⁴ Y. Kajiwara, K. Harii, S. Takahashi, J. Ohe, K. Uchida, M. Mizuguchi, H. Umezawa, H. Kawai, K. Ando, K. Takanashi, S. Maekawa, and E. Saitoh, Nature **464**, 262 (2010).

¹⁵ A. S. Nunez, R. A. Duine, P. Haney, and A. H. MacDonald, Phys. Rev. B **73**, 214426 (2006).

¹⁶ P. M. Haney and A. H. MacDonald, Phys. Rev. Lett. **100**, 196801 (2008).

¹⁷ Y. Xu, S. Wang, and K. Xia, Phys. Rev. Lett. **100**, 226602 (2008).

¹⁸ H. V. Gomonay and V. M. Loktev, Phys. Rev. B **81**, 144427 (2010).

¹⁹ J. Linder, Phys. Rev. B **84**, 094404 (2011).

²⁰ A. C. Swaving and R. A. Duine, Phys. Rev. B **83**, 054428 (2011).

²¹ K. M. D. Hals, Y. Tserkovnyak, and A. Brataas, Phys. Rev. Lett. **106**, 107206 (2011).

²² R. Cheng and Q. Niu, Phys. Rev. B **86**, 245118 (2012).

²³ E. G. Tveten, A. Qaiumzadeh, O. A. Tretiakov, and A. Brataas, Phys. Rev. Lett. **110**, 127208 (2013).

²⁴ A. Kapelrud and A. Brataas, Phys. Rev. Lett. **111**, 097602 (2013).

²⁵ R. Cheng and Q. Niu, Phys. Rev. B **89**, 081105 (2014).

²⁶ H. B. M. Saidaoui, A. Manchon, and X. Waintal, Phys. Rev. B **89**, 174430 (2014).

²⁷ R. Cheng, J. Xiao, Q. Niu, and A. Brataas, Phys. Rev. Lett. **113**, 057601 (2014).

²⁸ L. Onsager, Phys. Rev. **37**, 405 (1931).

- ²⁹ L. Onsager, Phys. Rev. **38**, 2265 (1931).
- ³⁰ F. M. Johnson and A. H. Nethercot, Phys. Rev. **114**, 705 (1959).
- ³¹ R. C. Ohlmann and M. Tinkham, Phys. Rev. **123**, 425 (1961).
- ³² M. Hagiwara, K. Katsumata, I. Yamada, and H. Suzuki, J. Phys.: Condens. Matter **8**, 7349 (1996).
- ³³ T. Wolfram and R. E. De Wames, Phys. Rev. **185**, 762 (1969).
- ³⁴ R. E. De Wames and T. Wolfram, Phys. Rev. **185**, 752 (1969).
- ³⁵ C. F. Osborne, J. Phys. C: Solid State Phys. **4**, 2354 (1971).
- ³⁶ F. Keffer and C. Kittel, Phys. Rev. **85**, 329 (1952).
- ³⁷ F. Keffer, American Journal of Physics **21**, 250 (1953).
- ³⁸ W. Marshall, Proceedings of the Royal Society of London. Series A, Mathematical and Physical Sciences **232**, 69 (1955).
- ³⁹ J. des Cloizeaux and J. J. Pearson, Phys. Rev. **128**, 2131 (1962).
- ⁴⁰ G. Roepke, Theor Math Phys **6**, 216 (1971).
- ⁴¹ J. Xiao and G. E. W. Bauer, Phys. Rev. Lett. **108**, 217204 (2012).
- ⁴² J. Xiao, A. Zangwill, and M. D. Stiles, Phys. Rev. B **72**, 014446 (2005).
- ⁴³ C. Kittel, *Introduction to solid state physics* (Wiley, 2005).
- ⁴⁴ D. Ködderitzsch, W. Hergert, W. M. Temmerman, Z. Szotek, A. Ernst, and H. Winter, Phys. Rev. B **66**, 064434 (2002).